Mathematical Theory and Modeling
ISSN 2224-5804 (Paper) ISSN 2225-0522 (Online)
Vol.7, No.6, 2017
www.iiste.org

Turbulent Natural Convection in an Enclosure at Varying Aspect Ratio

Stephen Karanja [1]*, Johana Sigey[2], Francis Gatheri[3], Eustace Kirima[4].

1.Department of Mathematics, Meru University of Science and Technology, P.O Box 972-60200, Meru, Kenya.

2. Department of Pure and Applied Mathematics, Jomo Kenyatta University of Agriculture and Technology, P.O Box 60000-00200, Nairobi, Kenya.

3. School of Mathematics and Actuarial Science, Technical University of Kenya, P.O Box 52428-00200, Nairobi,

Kenya.

4.Department of Mathematics, Meru University of Science and Technology, P.O Box 972-60200, Meru, Kenya.

Abstract

Energy transfer mechanism in most technical flows is through turbulent natural convection due to low viscosity of the fluids used in technical applications. Consequently, there is need to establish the parameters that influence the flow field of turbulent flow regime in order to enhance the energy-efficacy of many thermal applications. In order to establish the influence of the geometrical configuration of the flow domain on the flow field, we obtain and analyze the distribution of the velocity and temperature fields of a Boussinesq buoyancy-driven turbulent flow field in a locally heated and cooled enclosure for $0.5 \le AR \le 1$ while maintaining the Rayleigh number of the flow at 5.5×10^{10}. To filter out the enormous turbulent scales inherent in the turbulent flow regime, we decompose the flow variables present in the instantaneous equations governing a viscous Boussinesq buoyant flow and subject the resulting equations to the Reynolds averaging process to obtain equations that governs the turbulent flow field. We resolve the turbulent quantities emanating from this process using the $SST\, k-w$ turbulence model coupled with the Boussinesq approximation. To ensure the satisfaction of the conservation laws at the discrete level and over the entire solution domain, the non-dimensionalized equations are discretized using the robust finite volume method. The method possesses the ability to adapt a grid structure that captures the local features of the flow domain and imposes the integral form of the governing equations to each finite volume of the discretized solution domain so that the final mathematical formulation has an intimate connection to the actual physical situation. Since the equations are coupled, a segregated pressure-based iterative method is used to obtain the solution. The results revealed that the velocity and temperature fields are non-uniformly distributed in the enclosure and their magnitude and distribution significantly depend on the Aspect ratio of the enclosure. The results are consistent with the experimental results of Markatos and Pericleous (Markatos & Pericleous, 1984).

Keywords: Aspect Ratio, Boussinesq, Buoyancy, Natural Convection, Reynolds Stresses, Turbulent heat flux.

1.0 Introduction

There are two main mechanisms responsible for the transfer of heat in fluid flows. One is due to the random molecular movement of the fluid particles known as diffusion and the other is due to the macroscopic movement of fluid particles with the flow. However, in convective flows, heat transfer is predominantly due to the macroscopic movement of the fluid particles known as convection ((Rathakrishnan, 2005), (Bejan, 1984)). There are two processes in the convective mode of heat transfer, the forced and natural convection. If an external agent causes the movement of the fluid, the process is termed as forced convection. In this case, a superimposed external field is principally responsible for the fluid motion. The fluid motion is thus noticeable. On the other hand, whenever a surface in a fluid is at a temperature higher or lower than that of the fluid, the layer of the fluid in contact with the surface assumes the temperature of this surface through conduction. Due to temperature difference between this layer and the fluid particles within the vicinity, density gradient develops in the fluid. The presence of gravitational force in such a fluid induces buoyancy force that initiates fluid motion (Bergman & Incropera, 2011). The resulting fluid motion is termed as natural convection. In this case, the fluid motion is not noticeable since an internal condition causes the movement of the fluid particles. In natural convection, the flow rate is dependent on a non-dimensional number known as the Rayleigh number. Since the flow rate is a function of the coefficient of heat transfer, both the mechanism of heat transfer and the flow behavior are dependent of the Rayleigh number. When $Ra \le 10^4$, the mechanism of heat transfer is primarily by conduction whereas for $10^4 < Ra < 10^9$, laminar natural convection is the predominant mechanism of heat transfer. For $Ra \ge 10^9$, turbulent natural convection is the principal mechanism of heat transfer (Rajput, 2015). The coefficient of heat transfer of such flows is dependent on the fluid properties, the flow conditions and the geometry of the flow domain (Rajput, 2015). The Rayleigh number incorporates both the flow properties and flow conditions. Consequently, the behavior of a Boussinesq natural convective flow of constant Rayleigh number is dependent on the geometrical setup of the flow domain. However, most of the fluids used in technical applications are of low viscosity, hence, fluid flows encountered in technical applications are mostly turbulent. In order to meet the ever-increasing need of enhancing the energy-efficacy of many thermal systems, the determination of the influence of the Aspect ratio of the flow domain on the flow field of a turbulent natural convective flow is thus of great importance to the thermal science community.

Since the flow variables at a given point in a turbulent flow field exhibits a net mean behavior accompanied by rapid fluctuations about the mean, we subject the equations governing a Newtonian viscous Boussinesq buoyant flow to the Reynolds decomposition and averaging process in order to filter out the turbulent scales, moreover, we are interested with the gross behavior of the flow and thus equations that describe an average turbulent flow field will suffice (Patankar, 1980). The averaging process however introduces two unknown terms each in the momentum and energy equations associated with the fluctuations intrinsic in turbulent flow (Launder & Spalding, 1974). The determination of these terms poses the greatest challenge in the analysis of the turbulent flow field. In the present work, the Shear Stress Transport $k-w$ turbulence model developed (Menter, 1994) coupled with the Boussinesq approximation is used to model these terms.

1.1 Review of Previous Related Studies

Due to its many practical applications in the real world, the effect of the Aspect ratio of a flow domain on the flow field is receiving increasing research attention. Ganzarolli & Milanez, (1995) conducted a numerical study on natural convection in an enclosure heated from below and cooled symmetrically from the outside for $10^3 \le Ra < 10^9$. Results for $\Pr = 0.7$ and $\Pr = 0.67$ were obtained using the stream function-vorticity formulation. The Aspect ratio of the enclosure was varied between 1 and 9. The results comprised of isotherms and streamlines on different vertical planes and the Rayleigh-Nusselt number variations. They reported the effects of varying the Rayleigh number, Aspect ratio and the Prandtl Number of the fluid on heat transfer rate. (Sarris, Lekakis, & Vlachos, 2004) studied numerically natural convection in rectangular tanks heated locally from below. They investigated the effect of varying the geometry of the heated surface and the length of the tank on the flow patterns and heat transfer rates for Rayleigh number between 10^2 and 10^7. From the results, it was apparent that the intensity of the flow circulation increased with the width of the heated strip and the length of the tank.

Nogueira, Martins, & Ampessan, (2011) used computational fluid dynamics to analyze the effects of the Aspect ratio of the flow domain and the Rayleigh number of a natural convective flow on the rate of heat transfer and the flow profiles. The domain of analysis was a rectangular enclosure of different Aspect ratios. They considered $10^4 \le Ra \le 10^6$ and Enclosure Aspect ratio of 0.5, 1, 2 and 3. The results indicated that the distribution of the flow profiles, the rate of heat transfer and the thickness of the thermal boundary layer significantly depended on the Rayleigh number of the flow and the Aspect ratio of the enclosure. In addition, the results revealed that the average Nusselt number was a strong function of length to height ratio and increases with width to length ratio. During the same year, Gowda, Sridhara, & Seetharamu, (2011) used a finite volume based computational procedure to study the effect of the Aspect ratio on the flow profiles and heat transfer in the thermal boundary layer of the flow domain. The flow domain used for the analysis was a enclosure consisting of an adiabatic top wall, constant temperature cold vertical walls and a horizontal bottom subjected to uniform and linearly varying temperatures. Rayleigh number was ranged from 10^3 to 10^7 and the Aspect ratio of the enclosure from 0.5 to 3.0. From the results, whereas the Nusselt number for the bottom wall increased as the Aspect ratio increased from one to three, it decreased for the sidewalls. In addition, when they subjected the bottom wall to uniform temperature, the results revealed that the Nusselt number was higher than when subjected to linearly varying temperature.

(Falahat, 2014) investigated the influence of Aspect ratio and Rayleigh number on the Nusselt number in a laminar natural convection flow inside a water-filled square enclosure. The enclosure consisted of a partially heated vertical wall with the opposite vertical wall partially cooled. The top and bottom walls of the enclosure were both adiabatic. He solved the governing equations using the finite volume method for $10^3 \le Ra \le 10^6$ and $0.5 \le AR \le 4$. The results indicated that heat transfer enhances with increase of Rayleigh number for all Aspect ratios. However, the Nusselt number increases for Aspect ratio in the range of 0.5 to 1, beyond this range it decreases smoothly. (Salih, 2015) used the robust finite volume method on a collocated grid to investigate a steady two-dimensional laminar natural convection flow in a parallelogram shaped enclosure bounded by an

adiabatic top wall, constant temperature cold sidewalls and a hot bottom wall at uniform temperature. He considered velocity components and pressure as the dependent variables in the momentum equation. He used the SIMPLE algorithm to obtain the pressure field. The study considered Rayleigh number ranging from $10^3 \le Ra \le 10^5$ and $0.5 \le AR \le 1.5$. The results showed that the average Nusselt number increases as Aspect ratio and Rayleigh number increases. In addition, he asserted that the Aspect ratio of the flow domain is one of the most important parameters that determines the rate of heat transfer.

Most of the previous researches have considered the effect of the Aspect ratio on a laminar flow field. This paper documents the effect of the Aspect ratio on the distribution of the flow fields in a Boussinesq buoyancy-driven turbulent airflow in a locally heated and cooled enclosure with adiabatic walls.

2. Governing Equations

2.1 The Assumptions

The equations that govern Boussinesq buoyancy-driven turbulent flow result from invoking the laws of conservation of mass, momentum and energy. We however modify the momentum equation to incorporate the buoyancy term and neglect energy transfer through thermal conduction and radiation in the energy equation. Therefore, the derivation of the equations governing this flow regime is based on the premise that

- The fluid is Newtonian
- The flow is buoyancy-driven and turbulent.
- The dynamic and chaotic behavior inherent in turbulent flow does not violate the conservation laws
- All the flow variables are continuous functions of space
- Density is constant in the continuity equation and in all inertial terms in the momentum equation except in the buoyancy term.
- The heat transferred by conduction and radiation means is negligible.
- The viscous dissipation effects in the energy equation are negligible.
- The only body force acting on the fluid is gravity.
- Density gradients is purely as a result of temperature difference.

In a buoyant flow, a fluid of density ρ_0 displaces a fluid of density ρ, where ρ_0 is the reference fluid density and ρ is the instantaneous fluid density and $\rho < \rho_0$. This is due to buoyancy force caused by the imbalance between the gravitational and pressure forces acting on the fluid particles arising from density variations associated with temperature difference. A recirculating process thus characterizes buoyant flows. From Archimedes principle, the net force F_b acting on a unit mass of the fluid is

$$F_b = (\rho_0 - \rho)gV \tag{1}$$

Where V is the volume of the fluid displaced. But the volume of a unit mass of a fluid is

$$V = \frac{1}{\rho_0} \tag{2}$$

Hence

$$F_b = \frac{(\rho_0 - \rho)}{\rho_0} g \tag{3}$$

The density gradients that induces the buoyant force are due to temperature difference in fluid particles, thus, temperature is the primary variable in the flow. We thus express the buoyancy force in terms of temperature using the coefficient of volumetric expansion of the fluid. From definition, this coefficient is a measure of the rate of change of the volume of a fluid with temperature at constant pressure (Rajput, 2015)

$$\beta = \frac{1}{V_0}\left(\frac{\partial V}{\partial T}\right)_p \tag{4}$$

For a unit mass of a fluid, density is inversely proportional to the volume, therefore

$$\frac{1}{V_0}\left(\frac{\partial V}{\partial T}\right)_p = -\frac{1}{\rho_0}\left(\frac{\partial \rho}{\partial T}\right)_p \tag{5}$$

Thus, at constant pressure

$$\beta = -\frac{1}{\rho_0}\left(\frac{\Delta \rho}{\Delta T}\right) \tag{6}$$

It then follows that

$$\beta = -\frac{1}{\rho_o}\frac{(\rho - \rho_o)}{(T - T_o)} \tag{7}$$

Hence,

$$\frac{\rho_o - \rho}{\rho_o} = \beta\left[T - T_0\right] \tag{8}$$

Substituting equation (8) into (3) gives

$$F_b = g\beta\left[T - T_0\right] \tag{9}$$

It is apparent from equation (9) that the buoyancy force is a function of the coefficient of volumetric expansion of the fluid, the gravitational field strength and the temperature difference. Hence, for a Boussinesq fluid, buoyancy is purely a function of the temperature difference.

Considering a fluid flow with velocity component u_i in time t and spatial Cartesian co-ordinate x_i, the equations of continuity, momentum and energy respectively becomes (Currie, 2012)

$$\frac{\partial u_i}{\partial x_i} = 0 \tag{10}$$

$$\frac{\partial u_i}{\partial t} + u_j \frac{\partial u_i}{\partial x_j} = -\frac{1}{\rho_0}\frac{\partial p}{\partial x_i} + \nu \frac{\partial^2 u_i}{\partial x_j^2} + g_i\left[\beta(T - T_0)\right] \tag{11}$$

$$\frac{\partial T}{\partial t} + u_i \frac{\partial T}{\partial x_i} = \frac{k}{\rho c_p}\frac{\partial^2 T}{\partial x_i^{\,2}} \tag{12}$$

2.2 Decomposition and Averaging of the Conservation Equations

In order to incorporate the fluctuations that characterizes a turbulent flow, we subject equations (10) to (12) to the Reynolds decomposition and averaging process so that a flow variable ϕ is expressed as sum of a mean value and a fluctuation value as illustrated in the equation below

$$\phi(\mathrm{x},\mathrm{t}) = \bar{\phi}(\mathrm{x}) + \phi'(\mathrm{x},\mathrm{t}) \tag{13}$$

where ϕ denotes the instantaneous value of the variable whereas $\overline{\phi}$ and ϕ' denotes the associated mean and fluctuating value respectively. The mean value is determined by taking the time average of the variable over a long period compared with the time scale of a typical fluctuation as expressed in the equation below

$$\overline{\phi} = \lim_{\Delta t \to \infty} \int_{t}^{t+\Delta t} \phi(\mathrm{x,t}) dt \tag{14}$$

where Δt is the time averaging interval. Consequently, $\overline{\phi}$ does not change with time but with space.

We substitute the decomposed forms of the instantaneous variables present in equations (10) to (12) and subject the resulting equations to the Reynolds rules of averaging to obtain the time-averaged equations below

$$\frac{\partial \overline{u_i}}{\partial x_i} = 0 \tag{15}$$

$$\frac{\partial \bar{u}_i}{\partial t} + \bar{u}_j \frac{\partial \bar{u}_i}{\partial x_j} = -\frac{1}{\rho}\frac{\partial p}{\partial x_i} + g_i\left[\beta_0(\bar{T} - \bar{T}_0)\right] + \frac{\partial}{\partial x_j}\left[\mu \frac{\partial \bar{u}_i}{\partial x_i} - \rho \overline{u_i' u_j'}\right] \tag{16}$$

$$\rho c_p \frac{\partial \bar{T}}{\partial t} = -\frac{\partial}{\partial x_j}\left[-\kappa \frac{\partial \bar{T}}{\partial x_j} + \rho c_p \bar{u}_j \bar{T} + \rho c_p \overline{u_j' T'}\right] \tag{17}$$

The time-averaged equations (15) to (17) describes an average turbulent flow field. However, equation (16) and (17) contains unknown quantities $\rho \overline{u_i' u_j'}$ and $\rho \overline{u_j' T'}$ respectively. These terms referred to as turbulent stresses and turbulent heat flux respectively represents the additional transfer of momentum and energy due to the fluctuations in the turbulent flow.

3.0 MODELING THE TURBULENT QUANTITIES

3.1 The Boussinesq Approximation

Boussinesq postulated that turbulent stresses is linked to the mean strain rate through an apparent viscosity μ_t, whereas the turbulent heat flux is linked to the temperature gradient through an apparent coefficient of conduction k_t. This implies that, an average turbulent flow field is comparable to the corresponding laminar flow field (Versteeg & Malalasekera, 2007). However, both μ_t and k_t, unlike the laminar viscosity μ and thermal conductivity κ are not fluid properties but flow properties. Based on this analogy referred to as the Boussinesq approximation the turbulent stresses and the turbulent heat flux are expressed in terms of the mean strain rate and temperature gradients respectively as

$$\rho\,\overline{u_i' u_j'} = -\mu_t\left[\frac{\partial \bar{u}_i}{\partial x_j} + \frac{\partial \bar{u}_j}{\partial x_i}\right] + \frac{2}{3}\delta_{ij}\rho k \tag{18}$$

$$\rho\overline{u_i' T'} = -\frac{k_t}{c_p}\frac{\partial \bar{T}}{\partial x_i} \tag{19}$$

where k is the turbulent kinetic energy. The turbulent viscosity is a function of turbulent kinetic energy k and the turbulent scale length L (Rodi, 1993)

$$\mu_t = c_\mu \rho L\sqrt{k} \tag{20}$$

where c_μ is an empirical constant determined experimentally. Thus, to complete the model, we require an equation for the determination of turbulent kinetic energy and another equation that allows for the determination of the turbulent length scale.

3.2 Transport equations for the turbulent scalar quantities

3.2.1 Equation for Turbulent Kinetic Energy

This equation derived from the Navier-Stokes equation is of the form (Gatheri *et al.*, 1993)

$$\underbrace{\rho\frac{\partial k}{\partial t}}_{I} + \underbrace{\rho\bar{u}_j\frac{\partial k}{\partial x_j}}_{II} = \underbrace{-\rho\overline{u_i' u_j'}\frac{\partial u_i}{\partial x_j}}_{III} \underbrace{-\beta g\rho\overline{u' T'}}_{IV} - \frac{\partial}{\partial x_j}\left[\underbrace{\frac{1}{2}\rho\overline{u_i' u_i' u_j'}}_{V} + \underbrace{\overline{p' u_j'}}_{VI} - \underbrace{\mu\frac{\partial k}{\partial x_j}}_{VII}\right] \underbrace{-\mu\overline{\frac{\partial u_i'}{\partial x_j}\frac{\partial u_i'}{\partial x_j}}}_{VIII} \tag{21}$$

Each term in equation (21) represents an energy process occurring within the flow field. Apart from the terms *I, II* and *VII* representing the temporal, convection and molecular diffusion respectively, all other terms in the equation contains unknown correlations associated with the turbulent fluctuations. The correlations are modeled using similarity considerations coupled with the Boussinesq approximation as below.

Applying the Boussinesq approximation, the production term *III*, denoted as P_k becomes

$$P_k = -\rho\overline{u_i' u_j'}\frac{\partial \bar{u}_i}{\partial x_j} = \mu_t\left[\frac{\partial \bar{u}_i}{\partial x_j} + \frac{\partial \bar{u}_j}{\partial x_i}\right]\frac{\partial \bar{u}_i}{\partial x_j} - \frac{2}{3}\delta_{ij}\rho k\frac{\partial \bar{u}_i}{\partial x_j} \tag{22}$$

However, from the equation of continuity, $\frac{\partial \bar{u}_i}{\partial x_j} = 0.$ Equation (22) thus becomes

$$P_k = \mu_t \left[\frac{\partial \bar{u}_i}{\partial x_j} + \frac{\partial \bar{u}_j}{\partial x_i} \right] \frac{\partial \bar{u}_i}{\partial x_j} \tag{23}$$

Similarly, from equation (19), the buoyancy generation term IV , denoted by G_k becomes

$$G_k = -\beta g \rho \overline{u_i' T'} = \beta g \frac{k_t}{c_p} \frac{\partial \bar{T}}{\partial x_i} \tag{24}$$

But

$$k_t = \frac{\mu_t c_p}{\sigma_k} \tag{25}$$

Thus

$$G_k = \beta g \frac{\mu_t}{\sigma_k} \frac{\partial \bar{T}}{\partial x_i} \tag{26}$$

where σ_k is the turbulent Prandtl number.

The turbulent diffusion term v , is modeled using the assumption that kinetic energy diffuses down the gradient. The Fourier's law of heat flux supports this assumption. According to this law, heat diffuses from hot to cold regions (Rajput, 2015). Applying this law, we obtain

$$\frac{1}{2} \rho \overline{u_i' u_i' u_j'} = -\frac{\mu_t}{\sigma_k} \frac{\partial k}{\partial x_j} \tag{27}$$

The diffusion of turbulent kinetic energy due pressure gradient is small and consequently negligible. In addition, instead of modeling the turbulent dissipation term, an equation for its transport is developed.

Now using the modeled terms, we obtain the modeled equation for the transport of turbulent kinetic energy as

$$\rho \frac{\partial k}{\partial t} + \rho \bar{u}_j \frac{\partial k}{\partial x_j} = \frac{\partial}{\partial x_j} \left[\left(\mu + \frac{\mu_t}{\sigma_k} \right) \frac{\partial k}{\partial x_j} \right] + \mu_t \left[\frac{\partial \bar{u}_i}{\partial x_j} + \frac{\partial \bar{u}_j}{\partial x_i} \right] \frac{\partial \bar{u}_i}{\partial x_j} + \beta g \frac{\mu_t}{\sigma_k} \frac{\partial \bar{T}}{\partial x_i} - \mu \overline{\frac{\partial u_i'}{\partial x_j} \frac{\partial u_i'}{\partial x_j}} \tag{28}$$

3.2.2 Equation for the Turbulent Dissipation Term

From equation (28) for the transport of turbulent kinetic energy, the turbulent dissipation term is dependent on the descriptors of the large-scale motion k and L . The relation between these descriptors and the dissipation

rate is as given in the equation below

$$\varepsilon = c_d \frac{k^{\frac{3}{2}}}{L} \tag{29}$$

where c_d is an empirical constant. Rearrangement of equation (29) gives

$$L = \frac{c_d k^{\frac{3}{2}}}{\varepsilon} \tag{30}$$

Substituting equation (30) into (20) results into

$$\mu_t = c_\mu \frac{\rho k^2}{\varepsilon} \tag{31}$$

where c_μ is an empirical constant. From Wilcox (1998)

$$\varepsilon = \omega c_\mu k \tag{32}$$

where ω is the specific turbulent dissipation. This implies that

$$\mu_t = \frac{\rho k}{\omega}. \tag{33}$$

From the Wilcox formulation, the transport equation for ω is given as

$$\rho \frac{\partial \omega}{\partial t} + \rho \bar{u}_j \frac{\partial \omega}{\partial x_i} = \frac{\partial}{\partial x_j}\left[\left(\mu + \frac{\rho k}{\sigma_\omega \omega}\right)\frac{\partial \omega}{\partial x_i}\right] + \left[\beta - \frac{\kappa^2}{\sigma_\omega \sqrt{c_\mu}}\right]\rho \frac{\omega}{k} G_\omega - \rho \beta \omega^2. \tag{34}$$

Equations (28) and (34) provide the transport equations for the turbulent scalar quantities for the standard $k-\omega$ turbulence model. However, this model is sensitive in the freestream region.

3.3 The Modified Turbulent Transport Equations

On realizing the strengths and weaknesses of the standard turbulence models, Menter developed a blended model referred to as the Shear Stress Transport $k-\omega$ turbulence model to overcome the strong freestream sensitivity of the $k-\omega$ model in order to improve its predictions in regions with adverse pressure (Menter, 1994). He based its development on the results of physical experiments conducted to reveal flow behavior for engineering applications. The blended model switches to the $k-\omega$ turbulence model in the inner regions of the boundary

layer and transition regions and to $k-\varepsilon$ turbulence model in the freestream regions. Therefore, in order to adequately reveal the flow behavior in the entire flow domain, the $SST\ k-\omega$ turbulence model is the most appropriate model for resolving turbulence. The model is a variant of the $k-\omega$ model obtained by expressing the $k-\varepsilon$ model in terms of k and ω resulting into an additional term in the transport equation for ω called the cross-diffusion term defined as

$$D_{\omega} = 2[1-F_1]\rho\sigma_{\omega_{12}}\frac{1}{\omega}\frac{\partial k}{\partial x_j}\frac{\partial \omega}{\partial x_j} \tag{35}$$

where F_1 is a blending function. The turbulent viscosity of the model is obtained by modifying the turbulent viscosity term of the standard $k-\omega$ model given in equation (33) to include a term that make the model switch to $k-\varepsilon$ turbulence model in the freestream regions. The modified turbulent viscosity is as given in the equation below

$$\mu_t = \frac{\rho\alpha_1 k}{\max(\alpha_1\omega, \Omega F_2)} \tag{36}$$

where F_2 is a function defined as

$$F_2 = \tanh(\phi_2^2) \tag{37}$$

$$\phi_2 = \max\left[\frac{2\sqrt{k}}{C_\mu\omega}, \frac{500\mu}{\rho\omega y^2}\right]. \tag{38}$$

The first term in equation (36) originates from the definition of μ_t for a $k-\omega$ model while the second term vary with the normal distance from the boundary layer. This term reduces the turbulent viscosity in the regions where adverse pressure gradients are present thus enhancing the performance of the model.

The turbulent kinetic energy production term for the model is obtained using the equation below

$$G_k = \mu_t S^2 \tag{39}$$

S is the modulus of the mean strain rate tensor S_{ij}, defined as

$$S = \sqrt{2S_{ij}S_{ij}}. \tag{40}$$

and

$$S_{ij} = \sqrt{\frac{1}{2}\left[\frac{\partial u_i}{\partial x_j} + \frac{\partial u_j}{\partial x_i}\right]^2}. \tag{41}$$

The production term for ω is given by

$$G_\omega = \frac{\rho}{\mu_t}\alpha G_k \tag{42}$$

where

$$\alpha = \left|\frac{\alpha_\infty}{\alpha *}\left[\frac{\alpha_0 + \mathrm{Re}_t / R_w}{1 + \mathrm{Re}_t / R_w}\right]\right| \tag{43}$$

The dissipation rate of k and ω are respectively given as

$$\gamma_k = \rho\beta^* k\omega \tag{44}$$

$$\gamma_\omega = \rho\beta\omega^2 \tag{45}$$

Where

$$\beta^* = \beta_i^*\left[1 + \zeta^* F(m_t)\right] \tag{46}$$

and

$$\beta_i^* = \beta_\infty^*\left[\frac{\frac{4}{15} + \left[\frac{\mathrm{Re}_t}{R_\beta}\right]^4}{1 + \left[\frac{\mathrm{Re}_t}{R_\beta}\right]^4}\right]. \tag{47}$$

$F(m_t)$ is a compressibility function defined as,

$$F(m_t) = \begin{cases} 0, & m_t \le m_{t_0} \\ m_t^2 - m_{t_0}^2, & m_t \ge m_{t_0} \end{cases} \tag{48}$$

.

$$\left.\begin{aligned} m_t^2 &= \frac{2k}{a^2} \\ m_{t_0} &= 0.25 \\ a &= \sqrt{\gamma RT} \end{aligned}\right\} \tag{49}$$

$$\beta = \beta_i \left[1 - \frac{\beta_i^*}{\beta_i}\zeta^* F(m_t)\right] \tag{50}$$

$$\beta_i = F_1\beta_{i,1} + (1 - F_1)\beta_{i,2}. \tag{51}$$

The modified turbulent transport equations thus becomes:

Transport equation for turbulent kinetic energy k

$$\rho\frac{\partial k}{\partial t} + \rho\bar{u}_i\frac{\partial k}{\partial x_i} = \frac{\partial}{\partial x_j}\left[\left(\mu + \frac{\rho\alpha_1 k}{\sigma_k \max(\alpha_1\omega, \Omega F_2)}\right)\frac{\partial k}{\partial x_j}\right] + \frac{\rho^2 S^2 \alpha_1 k}{\sigma_k \max(\alpha_1\omega, \Omega F_2)} - \rho\beta^*\omega k \tag{52}$$

Transport equation for specific turbulent dissipation ω

$$\rho\frac{\partial \omega}{\partial t} + \rho\bar{u}_i\frac{\partial \omega}{\partial x_i} = \frac{\partial}{\partial x_j}\left[\left(\mu + \frac{\rho\alpha_1 k}{\sigma_\omega \max(\alpha_1\omega, \Omega F_2)}\right)\frac{\partial \omega}{\partial x_i}\right] + \left[\beta - \frac{\kappa^2}{\sigma_\omega\sqrt{c_\mu}}\right]\frac{\rho^2 S^2 \alpha_1 \omega}{\sigma_\omega \max(\alpha_1\omega, \Omega F_2)} + 2(1 - F_1)\rho\frac{\sigma_\omega}{\omega}\frac{\partial k}{\partial x_i}\frac{\partial \omega}{\partial x_i} - \rho\beta\omega^2 \tag{53}$$

The coefficients in the modified transport equations are blended forms of the standard $k-\varepsilon$ and $k-\omega$ models coefficients. The blended coefficients are obtained using the blending function F_1 defined as

$$F_1 = = \tanh\left[\phi_1^4\right] \tag{54}$$

where

$$\phi_1 = \min\left[\max\left(\frac{\sqrt{k}}{c_\mu\omega y}, \frac{500\mu}{\rho\omega y^2}\right), \frac{4\rho\sigma_{\omega 2}k}{CD_{K\omega}y^2}\right] \tag{55}$$

y is the normal distance to the wall and $CD_{K\omega}$ is the positive component of the cross-diffusion term defined as

$$CD_{K\omega} = \max\left[2\rho\sigma_{\omega 2} \frac{1}{\omega} \frac{\partial k}{\partial x_i} \frac{\partial \omega}{\partial x_i},\ 10^{-20} \right] \tag{56}$$

Accordingly, the blended coefficients are obtained using the relation below

$$\varphi = \varphi_1 F_1 + \varphi_2 (1 - F_1) \tag{57}$$

where φ is the blended coefficient, φ_1 is a coefficient from the standard $k-\omega$ model while φ_2 is the corresponding coefficient from the standard $k-\varepsilon$ model. The blended coefficients for the model are given in table 1 below.

Table 1: Coefficients for the $SST\, k-\omega$ model

$\sigma_{k,1}$	$\sigma_{k,2}$	$\sigma_{\omega,1}$	$\sigma_{\omega,2}$	α_1	α_∞^*	α_∞	α_0	$\beta_{i,1}$	$\beta_{i,2}$
1.176	1.0	2.0	1.168	0.31	1	0.52	1/9	0.075	0.0828

β_∞^*	R_β	R_k	R_ω	ζ^*	m_{t_0}	σ_k	σ_ω	C_μ	κ
0.09	8	6	2.95	1.5	0.25	2.0	2.0	0.09	0.41

3.4 *The Modeled Equations for an Average Turbulent Flow Field*

For clarity, the upper-case letters represent the mean-value component of the flow quantities while the lower-case letters represent the corresponding fluctuating component. For temperature, T represent the mean-value component while T represent the fluctuating component. Accordingly, the equations governing a Boussinesq buoyancy-driven mean turbulent flow field are

Equation of Continuity

$$\frac{\partial U_i}{\partial x_i} = 0 \tag{58}$$

Equation of Momentum

$$\frac{\partial U_i}{\partial t} + U_j \frac{\partial U_i}{\partial x_j} = -\frac{1}{\rho}\frac{\partial P}{\partial x_i} + g_i\left[\beta\left(T - T_0\right)\right] + \frac{\partial}{\partial x_j}\left[\mu\frac{\partial U_i}{\partial x_j} - \rho\overline{u_i u_j}\right] \tag{59}$$

Equation of Energy

$$\rho c_p \frac{\partial T}{\partial t} = -\frac{\partial}{\partial x_i}\left[-\kappa\frac{\partial T}{\partial x_j} + \rho c_p U_j T + \rho c_p \overline{u_j \mathrm{T}}\right] \tag{60}$$

Transport equation for turbulent kinetic energy

$$\rho\frac{\partial k}{\partial t} + \rho U_i \frac{\partial k}{\partial x_i} = \frac{\partial}{\partial x_j}\left[\left(\mu + \frac{\rho\alpha_1 k}{\sigma_k \max\left(\alpha_1\omega, \Omega F_2\right)}\right)\frac{\partial k}{\partial x_j}\right] + \frac{\rho^2 S^2 \alpha_1 k}{\sigma_k \max\left(\alpha_1\omega, \Omega F_2\right)} - \rho\beta^*\omega k \tag{61}$$

Transport equation for specific dissipation rate

$$\rho\frac{\partial \omega}{\partial t} + \rho U_i \frac{\partial \omega}{\partial x_i} = \frac{\partial}{\partial x_j}\left[\left(\mu + \frac{\rho\alpha_1 k}{\sigma_\omega \max\left(\alpha_1\omega, \Omega F_2\right)}\right)\frac{\partial \omega}{\partial x_i}\right] + \left[\beta - \frac{\kappa^2}{\sigma_\omega\sqrt{c_\mu}}\right]\frac{\rho^2 S^2 \alpha_1 \omega}{\sigma_\omega \max\left(\alpha_1\omega, \Omega F_2\right)} +$$
$$2\left(1 - F_1\right)\rho\frac{\sigma_\omega}{\omega}\frac{\partial k}{\partial x_i}\frac{\partial \omega}{\partial x_i} - \rho\beta\omega^2 \tag{62}$$

4.0 MATHEMATICAL FORMULATION

When the Rayleigh number of the flow is constant, the coefficient of heat transfer is dependent on the geometrical setup of the flow domain. This implies that the geometry of the flow domain affects the flow behavior. In order to establish the effect of the Aspect ratio of the flow domain on the flow field, we determine and analyze the distribution of velocity and temperature fields for a Boussinesq buoyancy-driven turbulent airflow of $Ra = 5.5\times10^{10}$ in a locally heated and cooled enclosure for $0.5 \le AR \le 1$ and $\mathrm{Pr} = 0.71$. The distribution of the flow field is revealed by the distribution of the velocity and temperature contours. Figure 1 below shows the physical set-up of the flow domain.

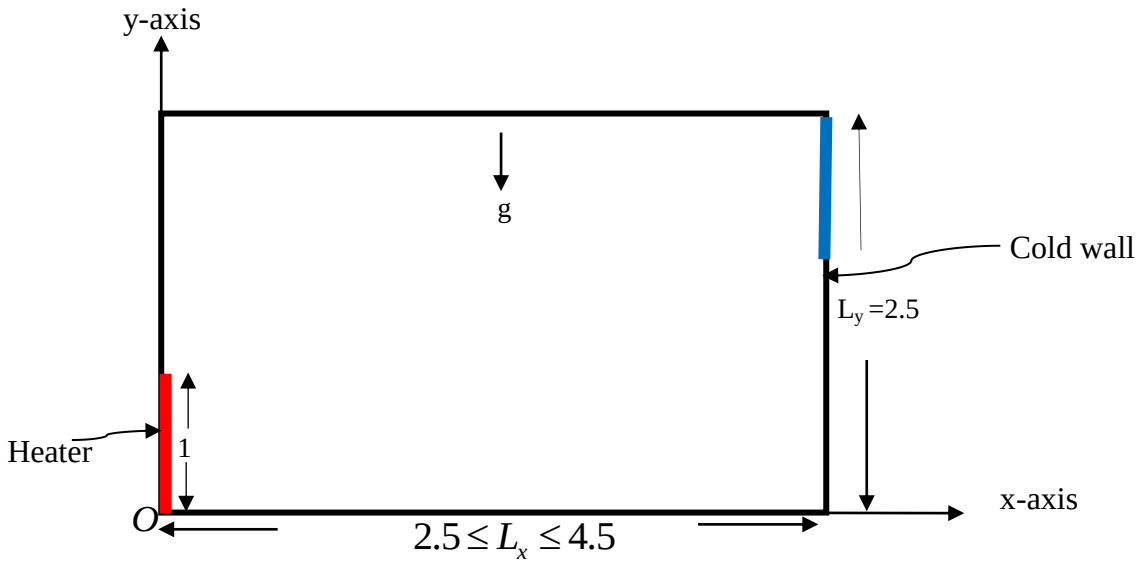

Figure 1: The physical set-up of the Enclosure

We define the Aspect ratio AR as the ratio of the convection height to a horizontal length of the flow domain. Accordingly, the Aspect ratio of the enclosure is defined in the equation below.

$$AR = \frac{L_y}{L_x} \tag{63}$$

From the figure, $L_y = 2.5$ whereas $2.5 \le L_x \le 4.5$, hence $0.5 \le AR \le 1$.

In order to reduce the number of variables in the governing equations we non-dimensionalize equations (58) to (62) using a non-dimensional scheme that combines several dimensionless variables into non-dimensional numbers that are significant to the prevailing flow conditions and ensures that the solution is bounded. Since the main goal is to find the value of u_i and T_i at position x_i in the enclosure, each of the flow variables is non-dimensionalized using a characteristic dimensionless variable in respect to the non-dimensional scheme proposed by Lankhorst in which the characteristic velocity U_* is defined as (Lankhorst & Marinus, 1991)

$$U_* = \frac{\lambda_0}{\rho_0 c_{p_0} l_0} \tag{64}$$

We further select l_0 and T_* as the characteristic length and temperature respectively. All other flow variables are non-dimensionalized by their respective values at temperature T_*. Accordingly, we introduce the following non-dimensional scaling variables in which the superscript prime denotes the non-dimensional quantities, the subscript star denotes a variable defined in respect to the non-dimensional scheme and the subscript 0 denotes

the variables evaluated at a reference state. The mean value and the corresponding fluctuation component of a variable share the same scaling variables

$$x_i^{'} = \frac{x_i}{l_0}\ ,\quad U_i^{'} = \frac{U_i}{U_*}\ ,\quad \nu^{'} = \frac{\nu}{\nu_0}\ ,\ \theta = \frac{T - T_*}{\Delta T_*},\ \rho^{'} = \frac{\rho}{\rho_0},\ k^{'} = \frac{k}{U_*}\ ,\ p^{'} = \frac{p}{p_0},\ \mu^{'} = \frac{\mu}{\mu_0}\ ,\ t^{'} = t\frac{U_*}{l_0}$$

$$g^{'} = \frac{g}{g_0} \tag{65}$$

Using this scheme, the non-dimensional form of equations (58) to (62) respectively becomes

$$\frac{\partial U_i}{\partial x_i} = 0 \tag{66}$$

$$\frac{\partial U_i}{\partial t} + U_j\frac{\partial U_i}{\partial x_j} = -\left(\frac{Ra\,\mathrm{Pr}^2}{\xi_\eta}\right)^{2/3}\frac{Pn}{Gn}\frac{1}{\rho}\frac{\partial P}{\partial x_i} + \left(\frac{Ra\,\mathrm{Pr}}{\xi_\eta}\right)(\beta\theta\Delta T_*) + \frac{\partial}{\partial x_j}\left[\mathrm{Pr}\,\nu\frac{\partial U_i}{\partial x_j} - \overline{u_i u_j}\right] \tag{67}$$

$$\rho c_p\frac{\partial\theta}{\partial t} = -\frac{\partial}{\partial x_i}\left[Pn\,\xi^{-1}\kappa\frac{\partial\theta}{\partial x_i} + \rho c_p U_i\theta + \rho c_p\overline{u_i\theta}\right] \tag{68}$$

$$\rho\frac{\partial k}{\partial t} + \rho U_j\frac{\partial k}{\partial x_i} = \mathrm{Pr}\frac{\partial}{\partial x_i}\left[\left(\mu + \frac{\rho\alpha_1 k}{\sigma_k\max\left(\alpha_1\omega,\Omega F_2\right)}\right)\frac{\partial k}{\partial x_i}\right] + \frac{Ra\,\mathrm{Pr}}{\xi_\eta}\left(\frac{\rho^2 S^2\alpha_1 k}{\max\left(\alpha_1\omega,\Omega F_2\right)}\right) - \rho\beta^*\omega k \tag{69}$$

$$\rho\frac{\partial\omega}{\partial t} + \rho U_j\frac{\partial\omega}{\partial x_i} = \mathrm{Pr}\frac{\partial}{\partial x_i}\left[\left(\mu + \frac{\rho\alpha_1 k}{\sigma_\omega\max\left(\alpha_1\omega,\Omega F_2\right)}\right)\frac{\partial\omega}{\partial x_i}\right] + \frac{Ra\,\mathrm{Pr}}{\xi_\eta}\frac{\omega}{k}\left[\beta - \frac{\kappa^2}{\sigma_\omega\sqrt{c_\mu}}\right]\left(\frac{\rho^2 S^2\alpha_1 k}{\max\left(\alpha_1\omega,\Omega F_2\right)}\right) - \beta\rho\omega^2 + \frac{1}{Gn}\left[\frac{Ra\,\mathrm{Pr}^2}{\xi_\eta}\right]^{2/3} 2(1-F_1)\frac{\sigma_\omega}{\omega}\frac{\partial k}{\partial x_i}\frac{\partial\omega}{\partial x_i} \tag{70}$$

Temperature boundary conditions

For a bounded solution, we bound the non-dimensional temperature $\theta = \frac{T - T_*}{\Delta T_*}$ within the flow domain. We conveniently choose $T_* = T_c$ so that on the heated region, $T = T_h$ hence,

$$\theta = \frac{T_h - T_c}{\Delta T_*} = \frac{T_h - T_c}{T_h - T_c} = 1. \tag{71}$$

On the cold region, $T = T_c$ hence

$$\theta = \frac{T_c - T_*}{\Delta T_*} = \frac{T_c - T_c}{T_h - T_c} = 0. \tag{72}$$

Thus within the enclosure, $0 \le \theta \le 1$.

The walls of the enclosure are adiabatic, thus taking n as a scalar of the outward unit vector normal to the walls,

. $$\frac{\partial \theta}{\partial n} = 0 \tag{73}$$

Velocity boundary conditions

The walls of the enclosure are stationary and impermeable. We specify the state of the fluid motion at the boundaries in terms of the velocity of the fluid particles. The non-slip velocity boundary condition apply on all the bounding surfaces of the enclosure as outlined below.

$$u\ (x=0,\ y,) = v\ (x=0,\ y) = 0 \tag{74}$$

$$u\ (x=L_x,\ y) = v\ (x= L_x,\ y)=0 \tag{75}$$

$$u\ (x,\ y = 0) = v\ (x,\ y = 0) = 0 \tag{76}$$

$$u\ (x,\ y = L_y) = v\ (x,\ y = L_y)=0 \tag{77}$$

However, the pressure field is not specified since it is deduced from the velocity field.

5. Numerical Method

Based on the assumption that a piecewise profile describing the variation of the dependent variable across neighbouring nodes exist, the solution domain is decomposed into a union of non-overlapping finite volumes whose centroids are the computational nodes. To ensure that the conservation laws are satisfied at both the local and global level, quantity balance of each dependent variable at each node of the computational domain is

determined using a generic conservation equation that comprises of all physical processes of transporting a quantity in the flow domain. We thus express each of the equations (66) to (70) in a conservative form as

$$\frac{\partial}{\partial t}\rho\phi+\left[\frac{\partial}{\partial x_j}(\rho u_j\phi)-\frac{\partial}{\partial x_j}\left(\Gamma_\phi\frac{\partial}{\partial x_j}\phi\right)\right]=S_\phi \tag{78}$$

where Γ_ϕ is the exchange coefficient of ϕ and S_ϕ is its source (Pinho, 2001). The equation contain four distinct terms. The first term on the left shows the change of the variable with time; the second term shows the advection of the variable with the flow whereas the third term shows the diffusion of the quantity. Both the second and third term thus represent the flux of ϕ across the boundaries of the finite volume. The term on the right hand side shows the source of the quantity. Consequently, the rate of change of ϕ in a finite volume with respect to time is equal to the sum of the net flux of ϕ due to convection into the finite volume, the net flux of ϕ due to diffusion into the finite volume and the generation rate of ϕ inside the finite volume (Douglas, Gasiorek, Swaffield, & Jack, 2005). The equation thus incorporates all the transport processes of a quantity and hence represents the flux balance in a finite volume. Therefore, by sequentially setting ϕ to $1, u, v, w, T, k \quad \omega$ and with the appropriate values of Γ_ϕ and S_ϕ, the equation of continuity, momentum, energy and the turbulent transport equations can all be written in the form of equation (78).

Integrating equation (78) over a finite volume, we obtain

$$\frac{\partial}{\partial t}\int_V \rho\phi\ dV+\int_V\frac{\partial}{\partial x_j}(\rho u_j\phi)dV-\int_V\frac{\partial}{\partial x_j}\left(\Gamma_\varphi\frac{\partial}{\partial x_j}\phi\right)dV=\int_V S_\phi\ dV\,. \tag{79}$$

Using the Gauss's divergence theorem, we convert the volume integrals in equation (79) into integrals over the entire surface S bounding the finite volume to obtain

$$\frac{\partial}{\partial t}\int_V(\rho\phi)dV+\left[\int_S(\rho\phi u)ds-\left(\Gamma_\phi\frac{\partial}{\partial x_j}\phi\right)ds\right]=\int_V S_\phi\ dV \tag{80}$$

The integrals are discretized using the finite volume method to obtain a system of algebraic equations of the form

$$a\phi+\sum_{nb}a_{nb}\phi_{nb}=b \tag{81}$$

The coefficient a contains the contributions of all the terms corresponding to ϕ. The coefficient a_{nb} contain the corresponding contributions of each of the neighbouring finite volumes whereas the coefficient b contains the contributions of the source terms. The SIMPLER algorithm is used to obtain the pressure field. Since each

finite volume provides one equation for each dependent variable, we obtain an equation set for each finite volume. However, these equations are coupled in sense that the coefficients in the equations depend on the previous values of the dependent variables. This implies that the coefficients are functions of the solution. Consequently, we use an iterative segregated pressure-based solver built in Fluent 16.0 that solves equations sequentially for each dependent variable. In each equation, the unknown is assumed to be a single field variable and hence the equation is solved without regard to the solution of other field variables. In order to improve the stability of the iteration process, we use under-relaxation factors to lower the variations of the dependent variable from one iteration to the next. The absolute residual measure of ϕ at a point in the computational domain is obtained using the equation below.

$$R = \left| a\phi - \sum_{nb} a_{nb}\phi_{nb} - b \right| \tag{82}$$

In every iteration, the value of the coefficients a_{nb} and b changes in each finite volume. The overall measure of the scaled residual in the entire computational domain thus becomes

$$R^{\phi} = \frac{\sum_{all\ cells} \left| a\ \phi - \sum_{nb} a_{nb}\phi_{nb} - b \right|}{\sum_{all\ cells} |a\ \phi|} \tag{83}$$

For convergence, we set $R^{\phi} \leq 10^{-6}$.

6. Results and Discussion

6.1 Validation of the results

For validation of the results, we compare the current results with the experimental results of Markatos & Pericleous, (1984) Figures 2 and 3 below respectively shows a comparison between the distribution of the velocity and temperature contours obtained in the current study at $Ra = 10^{10}$ and the Markatos and Pericleous experimental results at the same Rayleigh number.

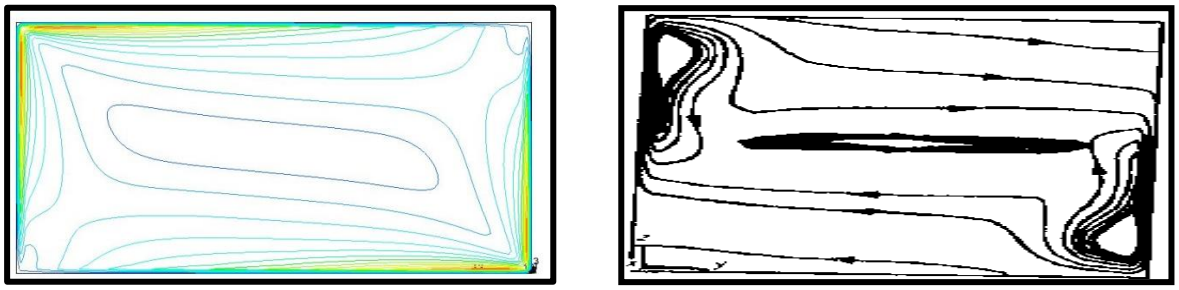

Current results **Markatos and Pericleous experimental results**

Figure 2: The distribution of velocity contours

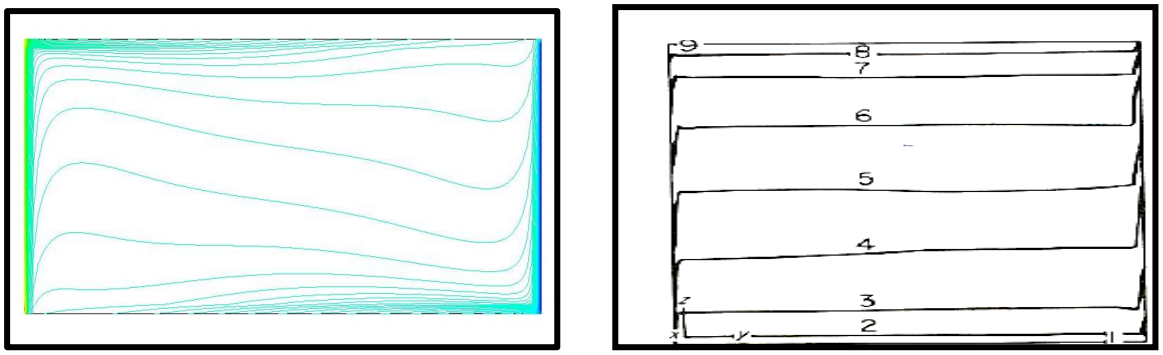

Current results

Markatos and Pericleous experimental results

Figure 3: The distribution of temperature contours

From figure 2, both results reveals the presence of recirculating vortices in the central region of the flow domain. It is also apparent from both results that velocity in the upper left and lower right regions of the flow domain is higher than the upper right and lower left regions. In addition, the results shows that the flow velocity is high in the regions near the heater and the cold wall while the interior is virtually stagnant. In both cases, the distribution of the velocity contours in the flow domain agree considerably. From figure 3, it is apparent from both results that the alignment of temperature contours is the same. In both cases, the temperature of the contours decrease gradually from the upper region of the flow domain to the lower side. Therefore, both results indicate that the flow domain is thermally stratified. Both results further reveals the existence of high temperature gradients along the vertical walls. This due to the effects of the buoyant forces. The results are therefore consistent with the experimental results. We therefore conclude that the results obtained satisfactorily reveals realistic flow behavior and hence are valid.

6.2 The distribution of velocity field in the Enclosure at different Aspect ratios

Figure 4 below shows the distribution of velocity contours in the enclosure at the indicated Aspect ratio.

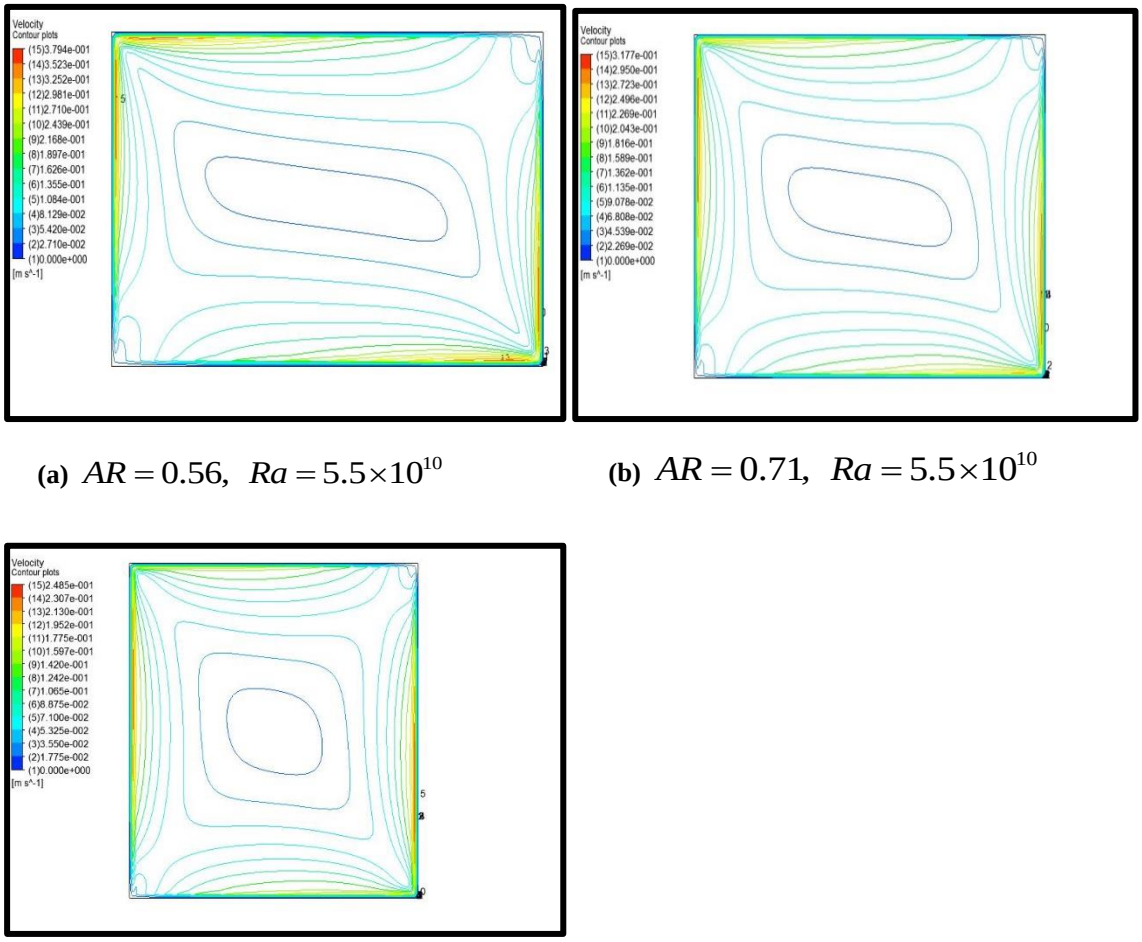

(a) $AR = 0.56,\ \ Ra = 5.5\times10^{10}$ **(b)** $AR = 0.71,\ \ Ra = 5.5\times10^{10}$

(c) $AR = 1,\ \ Ra = 5.5\times10^{10}$

Figure 4. The distribution of velocity contours in the enclosure

The distribution of the velocity contours provides a snapshot of the velocity field in the enclosure at the indicated values of the Aspect ratio. Therefore, the variation of the alignment of the velocity contours with the Aspect ratio as evidenced in figure 4 is a demonstration that the velocity field is dependent of the Aspect ratio of the flow domain. As the Aspect is increased from 0.5 to 1, the intensity of the velocity contours along the walls of the enclosure increases significantly leaving the central region with a low concentration of the velocity contours. These distributions depicts the distribution of kinetic energy in the enclosure at the specified Aspect ratio. It is also apparent from results that the distribution of the velocity of flow is high along the walls of the enclosure than the inner region. In addition, the flow velocity is generally high in the upper left and lower right hand regions of the enclosure whereas in the central region the velocity is low by one order of magnitude. Further, the velocity is low in the upper right and lower left regions of the enclosure, hence, the enclosure is velocity stratified. As the Aspect ratio increases, the alignment of the contours generally remains unchanged but the

magnitude of the flow velocity in the entire enclosure reduces significantly. Since the flow velocity is dependent on the buoyancy forces, we conclude that at constant Rayleigh number, distribution and the magnitude of the force that induces and sustains the flow is a function of the Aspect ratio of the flow domain. Therefore, for a confined convective flow, the velocity field is a function of the Aspect ratio of the flow domain.

6.3 The distribution of Temperature field in the Enclosure at different Aspect ratios

The influence of the Aspect ratio of the flow domain on the temperature field is revealed by the distribution of the temperature contours in the enclosure at the indicated values of the Aspect ratio as shown in the figure 5 below.

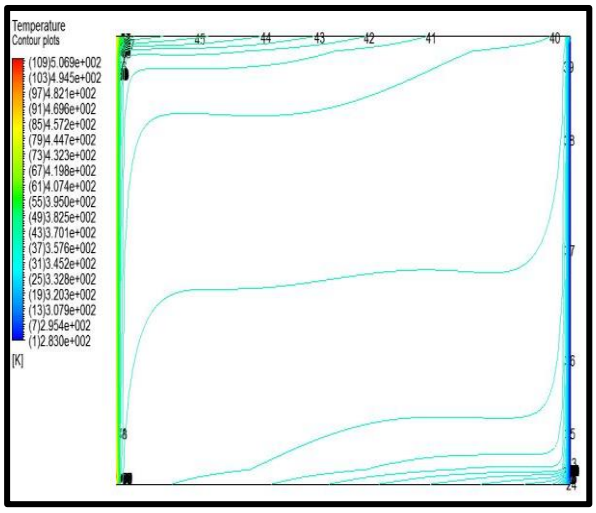

(a) $AR = 0.56,\ \ Ra = 5.5\times10^{10}$

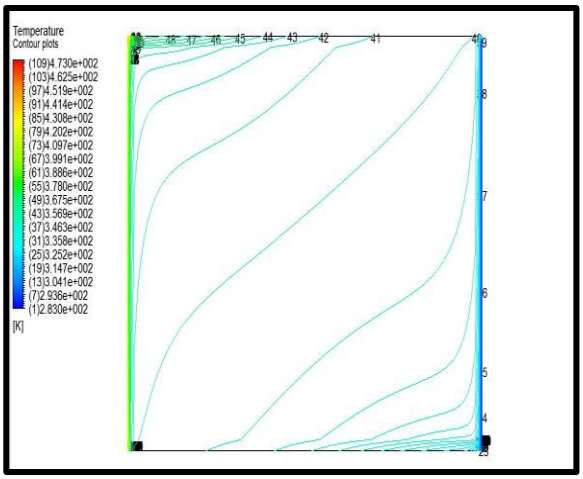

(b) $AR = 0.71,\ \ Ra = 5.5\times10^{10}$

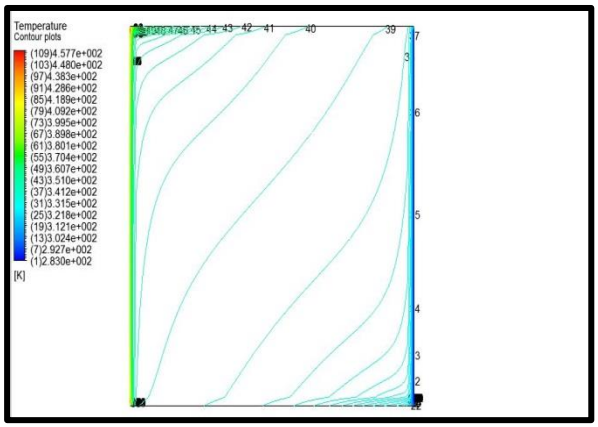

(c) $AR = 1,\ \ Ra = 5.5\times10^{10}$

Figure 5. The distribution of temperature contours in the enclosure

The results reveals that the magnitude and distribution of the temperature contours is dependent of the Aspect ratio of the enclosure. Generally, the upper region of the enclosure is at higher temperature than the lower region. However, the contours are highly concentrated in the upper left and lower right regions of the enclosure while in the central region the contours are sparsely distributed. As the Aspect ratio increases, the gradient of the contours increases significantly and they split into two sets. One set of the contours diverges towards the upper left corner while the other set diverges towards the lower right corner of the enclosure. The enclosure is thus stratified into three regions; the upper left region where the temperature is high, the lower right region where the temperature is low and the central region where the temperature is moderate. We thus conclude that at constant Rayleigh number, the temperature field is a strong of function of the Aspect ratio of the flow domain.

7.0 Conclusion

- At constant Rayleigh number, the magnitude of the buoyancy force is a function of the Aspect ratio of the flow domain.
- The Aspect ratio of a flow domain significantly influences both the distribution and the magnitude of the flow field.
- The thermal state of a confined flow domain is a function of its Aspect ratio.

8.0 Recommendations

- In the management of the thermal state of a confined flow domain, the Aspect ratio of the flow domain should be considered.
- Further research on the effect of the ratio of the heated area to cooled area on the distribution of the flow field to be conducted.

Nomenclature

Roman Symbols

AR	Aspect ratio of the flow domain
a_{nb}	Coefficients of the neighbouring finite volumes
C_p	Specific heat capacity at constant pressure
C_μ	Empirical turbulence constant
C_D	Cross-diffusion term

c_d	An empirical constant
$c_{\varepsilon 1}, c_{\varepsilon 2}$	Model constants
F	External body force per unit volume
F_b	Buoyancy force per unit volume
F_1	Blending functions
g	Acceleration due to gravitational
k	Turbulent Kinetic energy
k_t	Turbulent coefficient of conduction
G_k	Buoyant production of turbulent kinetic energy
P_k	Shear production of turbulent kinetic energy
L_0	Characteristic length of the convection
P	Thermodynamic Pressure
T	Thermodynamic Temperature
T_*	Characteristic Temperature
ΔT	Temperature difference
t	Time
Δt	Time interval
u_i	Instantaneous velocity components
U_i	Mean velocity components
U_*	Characteristic velocity
i, j	Unit vectors in the x, y directions respectively

L_x, L_y Dimensionless lengths of the flow domains in the x, y directions respectively

S Source term

d Diffusion term

n Normal vector

R Residual measure

Pr Prandtl number

Ra Rayleigh number

Gr Grashof number

Nu Nusselt number

Gn Gravity number

Greek Symbols

α Thermal diffusivity

β Co-efficient of volumetric expansion

ρ Density of fluid

ω Dissipation rate per unit of turbulent kinetic energy

μ Dynamic viscosity of the fluid

μ_t Turbulent viscosity

λ Thermal conductivity

θ Non-dimensional temperature

ε Dissipation rate of turbulent kinetic energy

ϕ A flow-field variable

φ Blended coefficients

γ_k, γ_ω Dissipation rate of k and ω respectively

κ	Coefficient of thermal conductivity of the medium
χ_i	Flux vector
ξ	Non-dimensional temperature difference
∂	Differential operator
σ_k	Turbulent Prandtl number for k

Subscripts

0	Reference state
h	Heater
t	Turbulent
nb	Neighbuor
*	Characteristic value

Superscripts

–	Mean value
'	Fluctuating component
'	Non-dimensional quantity
t	Time
m	Momentum equation
k	Turbulent kinetic energy equation
ω	Specific dissipation rate Equation

Acronyms

SIMPLER	SIMPLE Revised
CPU	Computer Processing Unit

Bibliography

Ahmadi, M. (2014). Fluid Flow and Heat Transfer Characteristics of Natural Convection in Square 3-D Enclosure Due to Discrete Sources. *World Applied Sciences Journal, 29*, 1291-1300. doi:10.5829/idosi.wasj.2014.29.10.1578

Ampofo, F., & Karayiannis, T. G. (2003). Experimental benchmark data for turbulent natural convection in an air filled square enclosure . *International Journal of Heat and Mass Transfer , 46*, 3551-3572. doi:http://dx.doi.org/10.1016/S0017-9310(03)00147-9

Anderson, J. (1995). *Computational Fluid Dynamics.* McGraw-Hill Education.

Aounallah, M., Addad, Y., Benhamadouche, S., Imine, O., Adjlout, L., & Laurence, D. (2007). *Numerical investigation of turbulent natural convection in an inclined square enclosure with a hot wavy wall.* Ph.D. dissertation. doi:http://dx.doi.org/10.1016/j.ijheatmasstransfer.2006.10.015

Awour, K. O. (2013). *Simulating Natural Turbulent Convection Fluid Flow in an Enclosure the Two-Equation Turbulent Models.* Ph.D. dissertation, Kenyatta University.

Aydin, O., & Yang, W.-J. (2000). Natural convection in enclosures with localized heating from below and symmetrical cooling from sides. *International Journal of Numerical Methods for Heat \& Fluid Flow, 10*, 518-529.

Bacharoudis, E., Vrachopoulos, M. G., Koukou, M. K., Margaris, D., Filios, A. E., & Mavrommatis, S. A. (2007). Study of the natural convection phenomena inside a wall solar chimney with one wall adiabatic and one wall under a heat flux . *Applied Thermal Engineering , 27*, 2266-2275. doi:http://dx.doi.org/10.1016/j.applthermaleng.2007.01.021

Bejan, A. (1984). *Convection Heat Transfer.* Wiley.

Bergman, T. L., & Incropera, F. P. (2011). *Introduction to Heat Transfer.* Wiley.

Blazek, J. (2001). *Computational Fluid Dynamics: Principles and Applications.* Elsevier Science.

Boussinesq, J. (1903). *Theorie analytique de la Chaleur.* Gauthier-Villars.

Cebeci, T., & Smith, A. M. (1974). *Analysis of turbulent boundary layers.* Academic Press, Incorporated.

Churchill, S. W., & Usagi, R. (1972). A general expression for the correlation of rates of transfer and other phenomena. *AIChE Journal, 18*, 1121-1128. doi:10.1002/aic.690180606

Currie, I. G. (2012). *Fundamental Mechanics of Fluids, Fourth Edition.* Taylor & Francis.

Davidson, L. (2011). *An Introduction to Turbulence Models.* Chalmers University of Technology.

de Vahl Davis, G. (1986). Finite difference methods for natural and mixed convection in enclosures. *Proceedings in the 8th International Heat Transfer Conference, 1*, pp. 101-109.

De Vahl Davis, G., Leornard, E., & Wong, S. A. (1988). *Three-dimensional natural convection in a room.* Tech. rep., University of New South Wales, Sidney.

Dol, H. S., & Hanjalić, K. (2001). Computational study of turbulent natural convection in a side-heated near-cubic enclosure at a high Rayleigh number . *International Journal of Heat and Mass Transfer , 44*, 2323-2344. doi:http://dx.doi.org/10.1016/S0017-9310(00)00271-4

Douglas, J. F., Gasiorek, J. M., Swaffield, J. A., & Jack, L. B. (2005). *Fluid Mechanics.* Pearson/Prentice Hall.

Falahat, A. (2014). Effect of Aspect Ratio on Laminar Natural Convection in Partially Heated Enclosure. *Universal Journal of Mechanical Engineering, 2*, 28-33.

Ferziger, J. H., & Peric, M. (2012). *Computational Methods for Fluid Dynamics.* Springer Berlin Heidelberg.

Ganzarolli, M. M., & Milanez, L. F. (1995). Natural convection in rectangular enclosures heated from below and symmetrically cooled from the sides. *International Journal of Heat and Mass Transfer, 38*, 1063-1073. doi:http://dx.doi.org/10.1016/0017-9310(94)00217-J

Gatheri, F. K., Reizes, J. A., Leonardi, E., & De Vahl Davis, G. (1993). Natural Convection in a Rectangular Enclosure with Colliding Boundary Layers: Numerical study. *Proceedings 5th Australasian Heat and Mass Conference*, 69.1-69.6.

Gowda, G. a., Sridhara, S. N., & Seetharamu, K. N. (2011). Effect of different thermal boundary conditions at bottom wall on natural convection in cavities. *Journal of Engineering Science and Technology, 6*, 109-130.

Hinze, J. O. (1975). *Turbulence: .* McGraw-Hill.

Kulkarni, R. (1998). Natural convection in enclosures with localised heating and cooling. *Doctor of Philosophy thesis, Department of Mechanical Engineering, University of Wollongong*.

Kundu, P. K., & Cohen, I. M. (2001). *Fluid Mechanics.* Elsevier Science.

Lankhorst, A. M., & Marinus, A. (1991). Laminar and turbulent convection in cavities: Numerical modeling and experimental validation. *Ph.D. Thesis Technische Univ., Delft (Netherlands).*

Launder, B. E., & Spalding, D. B. (1974). The numerical computation of turbulent flows. *Computer Methods in Applied Mechanics and Engineering, 3*, 269-289. doi:http://dx.doi.org/10.1016/0045-7825(74)90029-2

Mairura, O. E., Sigey, J. K., Okello, J. A., & Okwoyo, J. M. (2013). Natural Convection with Localized Heating and Cooling on Opposite Vertical Walls in an Enclosure. *The SIJ Transactions on Computer Networks \& Communication Engineering (CNCE)*.

Markatos, N. C., & Pericleous, K. A. (1984). Laminar and turbulent natural convection in an enclosed enclosure. *International Journal of Heat and Mass Transfer, 27*, 755-772. doi:http://dx.doi.org/10.1016/0017-9310(84)90145-5

Menter, F. R. (1994, #aug#). Two-equation eddy-viscosity turbulence models for engineering applications. *AIAA Journal, 32*, 1598-1605. doi:10.2514/3.12149

Monin, A. S., & Yaglom, A. M. (2007). *Statistical Fluid Mechanics: Mechanics of Turbulence* (illustrated, reprint ed.). Dover Publications.

Nogueira, R. M., Martins, M. A., & Ampessan, F. (2011). Natural convection in rectangular cavities with different Aspect ratios. *Science Engenharia T{\'{e}}rmica (Thermal Engineering), 44*, 1-2.

November, M., & Nansteel, M. W. (1987). Natural convection in rectangular enclosures heated from below and cooled along one side. *International Journal of Heat and Mass Transfer, 30*, 2433-2440. doi:http://dx.doi.org/10.1016/0017-9310(87)90233-X

Omri, M., & Galanis, N. (2007). Numerical analysis of turbulent buoyant flows in enclosures: Influence of grid and boundary conditions. *International Journal of Thermal Sciences, 46*, 727-738. doi:http://dx.doi.org/10.1016/j.ijthermalsci.2006.10.006

Onyango, M. O., Sigey, K. J., Okelo, A. J., & Okwoyo, M. J. (2013). Enhancement of Natural Convection Heat Transfer in a Square Enclosure with Localized Heating from Below. *International Journal of Science and Research, 2*.

Ozoe, H., Mouri, A., Hiramitsu, M., Churchill, S. W., & Lior, N. (1986, nov). Numerical Calculation of Three-Dimensional Turbulent Natural Convection in a Cubical Enclosure Using a Two-Equation Model for Turbulence. *Journal of Heat Transfer, 108*, 806-813.

Ozoe, H., Mouri, A., Ohmuro, M., Churchill, S. W., & Lior, N. (1985). Numerical calculations of laminar and turbulent natural convection in water in rectangular channels heated and cooled isothermally on the opposing vertical walls. *International Journal of Heat and Mass Transfer, 28*, 125-138. doi:http://dx.doi.org/10.1016/0017-9310(85)90014-6

Paolucci, S., & Chenoweth, D. R. (1989). Transition to chaos in a differentially heated vertical enclosure. *Journal of Fluid Mechanics, 201*, 379-410.

Patankar, S. (1980). *Numerical Heat Transfer and Fluid Flow.* Taylor & Francis.

Peng, S.-H., & Davidson, L. (1999). Computation of turbulent buoyant flows in enclosures with low-Reynolds-number k-omega models. *International Journal of Heat and Fluid Flow , 20*, 172-184. doi:http://dx.doi.org/10.1016/S0142-727X(98)10050-4

Peng, S.-H., & Davidson, L. (2001). Large eddy simulation for turbulent buoyant flow in a confined enclosure . *International Journal of Heat and Fluid Flow , 22*, 323-331. doi:http://dx.doi.org/10.1016/S0142-727X(01)00095-9

Pinho, F. T. (2001). The Finite-volume Method Applied to Computational Rheology: II-Fundamentals for Stress-explicit Fluids. *University of Porto, 1*, 63-100.

Pletcher, R. H., Tannehill, J. C., & Anderson, D. (2016). *Computational Fluid Mechanics and Heat Transfer, Third Edition.* CRC Press.

Rajput, R. K. (2015). *Heat and Mass Transfer: A Textbook for the Students Preparing for B.E., B.Tech., B.Sc. Engg, AMIE, UPSC (Engg. Services) and GATE Examinations.* S. Chand Limited.

Rathakrishnan, E. (2005). *Fundamentals of engineering thermodynamics.* PHI Learning.

Rodi, W. (1993). *Turbulence Models and Their Application in Hydraulics.* Taylor & Francis.

Sadowski, D., Poulikakos, D., & Kazmierczak, M. (1988, jul). Three-Dimensional Natural Convection Experiments in an Enclosure. *Journal of Thermophysics and Heat Transfer, 2*, 242-249. doi:10.2514/3.56223

Sajjadi, H., Gorji, M., Hosseinizadeh, S. F., Kefayati, G. R., & Ganji, D. D. (2011). NUMERICAL ANALYSIS OF TURBULENT NATURAL CONVECTION IN SQUARE ENCLOSURE USING LARGE-EDDY SIMULATION IN LATTICE BOLTZMANN METHOD. *Transactions of Mechanical Engineering, 35*, 133-142.

Salih, E. A. (2015). Effects of Aspect Ratio on Natural Convection Heat Transfer in a Parallelogrammic Enclosure Heated from Below. *ZANCO Journal of Pure and Applied Sciences, 27*, 45-56.

Sarris, I. E., Lekakis, I., & Vlachos, N. S. (2004). Natural convection in rectangular tanks heated locally from below . *International Journal of Heat and Mass Transfer , 47*, 3549-3563. doi:http://dx.doi.org/10.1016/j.ijheatmasstransfer.2003.12.022

Sharif, M. L., & Mohammed, L. A. (2005). Unsteady free convection and mass transfer in rectangular cavities using the finite volume based computational method. *Thermal International Journal, 10*, 568-789.

Sigey, J. K., Gatheri, F. K., & Kinyanjui, M. (2004). Numerical study of free convection turbulent heat transfer in an enclosure . *Energy Conversion and Management , 45*, 2571-2582. doi:http://dx.doi.org/10.1016/j.enconman.2003.10.010

Sodja, J. (2007). *Turbulence models in CFD.* University of Ljubljana.

Tennekes, H., & Lumley, J. L. (1972). *A First Course in Turbulence.* Pe Men Book Company.

Versteeg, H. K., & Malalasekera, W. (2007). *An Introduction to Computational Fluid Dynamics: The Finite Volume Method.* Pearson Education Limited.

Wilcox, D. C., & others. (1998). *Turbulence modeling for CFD* (Vol. 2). DCW industries La Canada, CA.